Supporting Information

Structure-Stability-Function Mechanistic Links in the Anti-Measles Virus Action of Tocopherol-Derivatized Peptide Nanoparticles

Tiago N. Figueira[1], Diogo A. Mendonça[1], Diana Gaspar[1], Manuel N. Melo[2], Anne Moscona[3,4,5,6], Matteo Porotto[3,4,7], Miguel A.R.B. Castanho[1]*, Ana Salomé Veiga[1]*

[1]Instituto de Medicina Molecular, Faculdade de Medicina, Universidade de Lisboa, 1649-028 Lisbon, Portugal
[2]Instituto de Tecnologia Química e Biológica António Xavier, Universidade Nova de Lisboa, 2775-412 Oeiras, Portugal
[3]Department of Pediatrics, Columbia University Medical Center, NY 10032, United States
[4]Center for Host-Pathogen Interaction, Columbia University Medical Center, NY 10032, United States
[5]Department of Microbiology & Immunology, Columbia University Medical Center, NY 10032, United States
[6]Department of Physiology & Cellular Biophysics, Columbia University Medical Center, NY 10032, United States
[7]Department of Experimental Medicine, University of Campania 'Luigi Vanvitelli', 81100 Caserta, Italy

Peptides description and molecular structure

The measles virus (MV)-specific antiviral peptides studied in the present work share a common 42 amino acid residues sequence (Fig. S1, A and B). This core sequence is composed by a 36-mer segment derived from the MV F envelope glycoprotein C-terminal heptad repeat (HRC, residues 450-485), previously identified as a potent MV fusion inhibitor,[1] extended with a GSGSGC spacer motif.

The C-terminal cysteine residue was used for chemical conjugation with polyethylene glycol (PEG)/tocopherol (Toc) tags, by means of thiol-reactive reagents. Derivatization with hydrophobic moieties consists in a general strategy for improvement of peptide fusion inhibitor properties,[2] associated with both peptide self-association and lipid membrane partition.[3] A bromoacetylated and tetrameric PEG (PEG_4)-Toc reagent was used to prepare a Toc-tagged monomeric peptide, HRC5 (Fig. S1, C). Also, a bis-maleimide (MAL) functionalized PEG_4-Toc reagent with double PEG_4 configuration ($[MAL\text{-}PEG_4]_2$-Toc) was used to prepare the equivalent Toc-tagged dimeric peptide, HRC6 (Fig. S1, D). A 1:1 and 1:2 stoichiometry conjugation reaction between reagents and the core peptide sequence was carried out for HRC5 and HRC6, respectively. The unconjugated core sequence was used as a control peptide, HRC1. In this case, the cysteine was blocked through iodoacetamine alkylation to avoid disulphide bond formation between peptides.

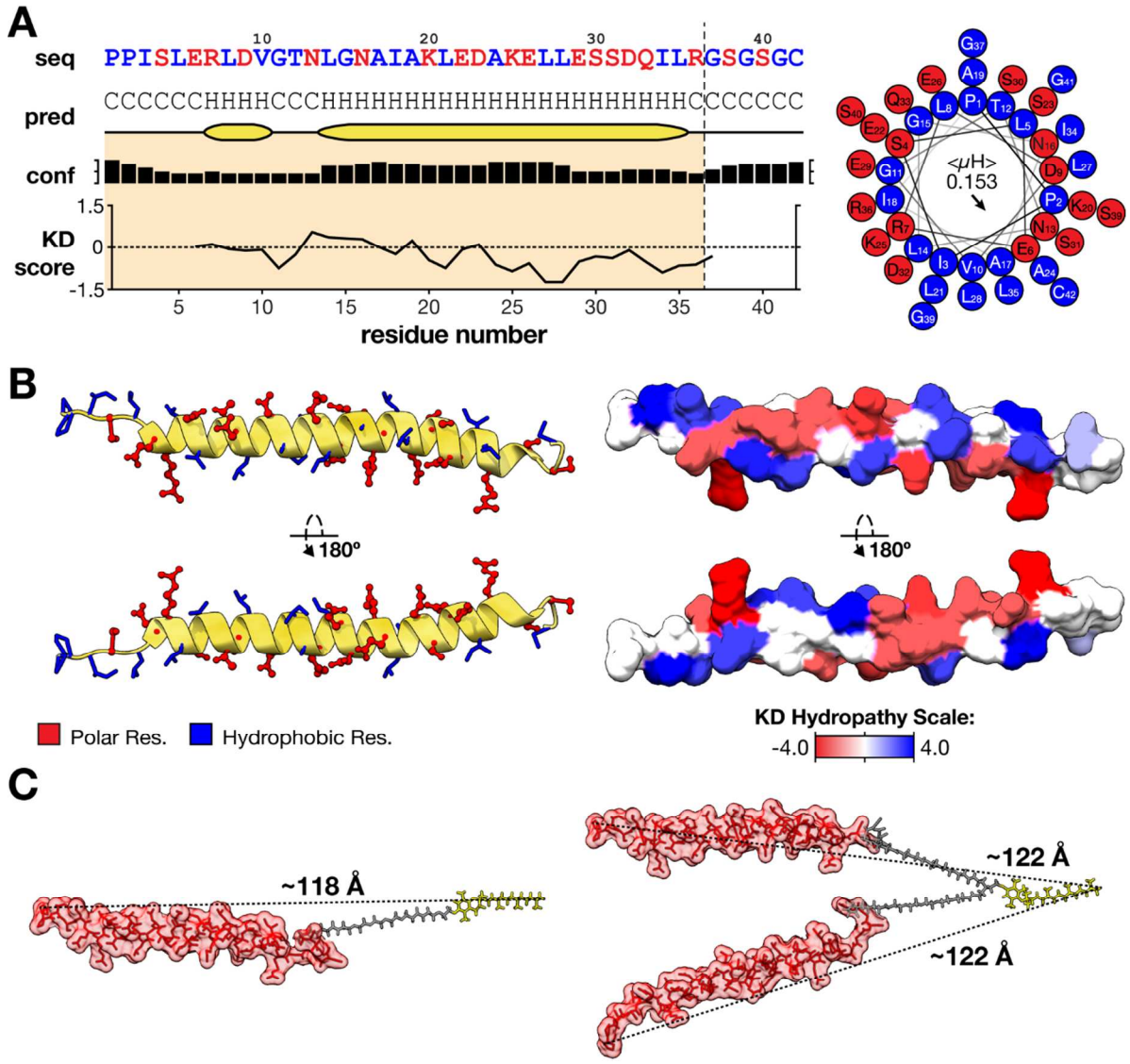

Figure S1 – MV-specific antiviral peptides sequence and structural features. (A) Antiviral peptides common core sequence composed by a MV F HRC-derived segment (residues 1-36) and spacer motif (residues 37-42) is represented in single letter code. Polar and hydrophobic amino acid residues are highlighted in red and blue, respectively. Sequence-based secondary structure predictions and respective confidence levels were obtained through the PSIPRED online server.[4,5] 26 out of 42 amino acid residues contribute to peptides α-helical conformation. Predicted random coil and α-helix regions are depicted as "C"/full lines and "H"/orange boxes, respectively. The Kyte-Doolitle (KD) sequence-dependent hydropathy profile, indicating peptides hydrophilic nature, was determined through the ExPaSy ProtScale webtool, using 11 amino acid residues intervals.[6] Peptide α-helix wheel projection adapted from HELIQUEST analysis web server[7] outputs suggest low helical amphipathicity. The representation is oriented from the peptide N- to C-terminus and includes the theoretical mean hydrophobic moment, <μH>, and respective moment orientation. **(B)** Homology-based simulation of the MV-specific antiviral peptide 3D molecular structure obtained through the I-TASSER online server.[8-10] PDB entry 1ZTM was

used as homology template for structural predictions. Antiparallel 3D representations emphasizing peptide secondary structure and amino acid residues (left) as well as the Kyte-Doolitle hydropathy surface profile (right) were prepared using the UCSF Chimera molecular modelling software.[11] **(C)** 3D representations of HRC5 (left) and HRC6 (right) peptides assembled through the Avogadro software.[12] Peptide molecules were built from the homology-predicted amino acid sequence structure (red), represented in B, complemented with the remaining chemically conjugated domains: flexible PEG_4 linker (grey) and Toc moiety (yellow). The presented structures were stabilized through energy minimization calculations. Peptides longitudinal axis dimensions are included.

Coarse-grained tocopherol model development and validation

The lack of available Toc coarse-grained (CG) topology in known libraries or publications, prompted the development of a novel CG model for Toc. Reference fine-grained (FG) structural data was obtained using automatically-generated atomistic models from the ATB server (Molecule ID 20731), for use with the GROMOS 54a7 force field.[13] FG simulation data was used to estimate bonded parameters for the CG model. The general FG simulation conditions are described elsewhere.[14]

The strategy for Toc CG model building consisted in a 5:1 mapping of the tail, composed by 3 beads – C1 to C3, followed by a virtual site approach employed for the head:[15] the double-ring head was built as a rigid body by constraining the distances between beads R4, R2 and R3 and defining bead R1 as a virtual interaction site constructed from the other three beads (Fig. S1). The R2–R3, R2–R4, and R3–R4 distances were constrained. The virtual site at R1 was built in the plane of the R4–R2–R3 frame, with parameters a = 1.12915 and b = 0.77212. and was excluded from nonbonded interactions with it (see ref. [14] for further examples of such virtual-site usage). The remaining R4–C1, C1–C2, and C2–C3 bonds were modelled by harmonic restraints. Angle potentials, of the cosine-harmonic type, were placed on the ring–tail hinge, and on the tail itself. A single cosine dihedral angle restraint of multiplicity 1 was used for ring–tail orientation, over beads R2–R3–R4–C1. Because of instability brought about by this restraint when beads R3–R4–C1 become collinear, an extra angle potential was placed on those beads to keep them from collinearity.[16] The potential parameters are summarized in Table S1, and comparison of the relevant generated distributions is presented in Fig. S1-C, showing an overall good agreement.

Table S1 – Bonded parameters of the CG Toc model

	Beads	Equilibrium value[1]	Force constant[2]
Constraints	R2–R3	0.333	
	R2–R4	0.325	
	R3–R4	0.390	
Bonds	R4–C1	0.43	5000
	C1–C2	0.47	1500
	C2–C3	0.47	1500
Angles	R3–R4–C1	113	20
	R3–R4–C1[3]	113	10
	R4–C1–C2	100	25
	C1–C2–C3	120	25
Dihedral	R2–R3–R4–C1	-55	50

[1] Equilibrium value units are nm for constraints and bonds, and degrees for angles and dihedrals.

[2] Force constant units are in kJ/mol/nm^2 for bonds and kJ/mol for angles and dihedrals.

[3] A restricted bending potential was overlaid on these atoms at the same equilibrium value as the cosine-harmonic angle.

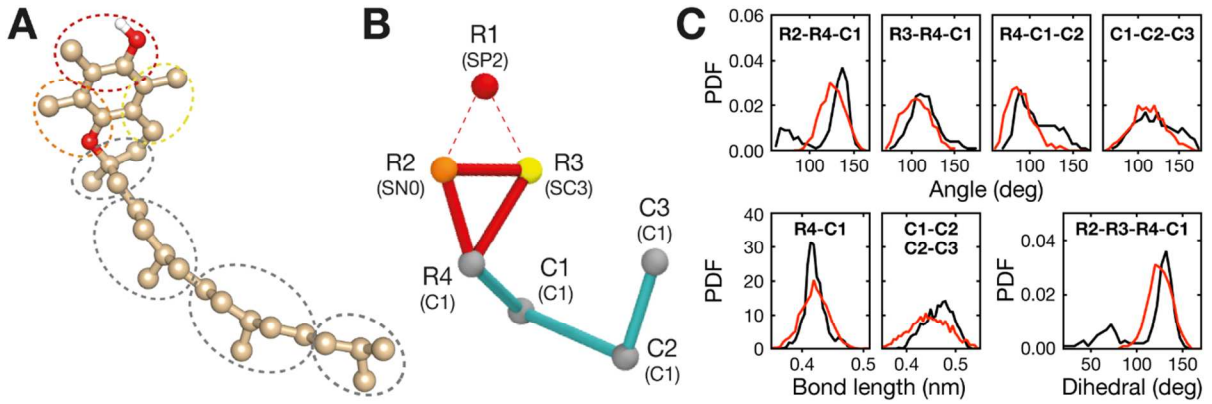

Figure S2 – Simulated Toc structures. (A) Rational schematics used for the Toc CG model construction from the Toc atomistic structure. The dotted lines separate the atom groups used for the CG model shown in panel B; mapping was done by the center-of-mass of each group, discarding hydrogens. (B) CG model for Toc with application of the virtual site approach. The CG bead names, and particle types in parenthesis,[17] are overlaid in the image. (C) Comparison of bonded structural parameters between the mapped FG reference configurations (black lines) and the CG model (red lines), expressed as a probability density function (PDF). Note that not all the angles compared here were restrained in the topology.

For the Toc model parameterization, CG data was generated with the Martini model and simulated at 20 fs integration steps. Standard Martini Lennard-Jones and Coulomb potentials[17] were used and neighbour list updates were performed every 20 steps. Temperature was coupled to 300 K using the v-rescale[18] thermostat, with a 1 ps coupling time. Pressure was isotopically coupled to 1 bar using the Berendsen barostat[19] with a 3 ps coupling time. The tuning of Toc CG bonded parameters (the stiffness of the bonds, angles and dihedrals) was done by trial and error of different potential combinations against the FG reference system. This repeated testing was performed in standard Martini water.[17]

Octanol-water partition was used to validate the proposed bead type assignments of the CG Toc model.[20] Free-energies were calculated from the individual solvation free-energies into each solvent. The same run parameters were used for parameterization, while pressure was coupled using the Parrinello-Rahman barostat[19] with 12 ps coupling time. Single Toc molecules were decoupled from solvent boxes of either 1618 Martini waters or 614 octanol molecules plus 52 Martini waters (corresponding to a water-saturated octanol phase). Decoupling was performed in 10 steps of 10 ns each, by scaling down solute-solvent Lennard-Jones interactions. Free-energy values were obtained by the MBAR approach.[20] Octanol/water partition free-energy values correspond to the difference between solvation free energy in water and solvation free-energy in octanol, used to determine partition coefficient (K_p) through the equation:

$$\Delta G = 2.303 \times K_B \, T \log_{10}(K_p) \quad \text{(S1)}$$

where, ΔG is the octanol/water partition free-energy, K_B is Boltzmann constant, T the temperature and K_p the partition coefficient. Octanol/water partition free-energy for Toc CG model was 45.52 ± 0.63 J/mol, which is equivalent to a $\log_{10}(K_p)$ = 7.925 ± 0.11. Listed experimental and predicted values for Toc $\log_{10}(K_p)$ range from 8.84 to 10.51 (www.drugbank.ca, accession number DB00163; no source for the experimental $\log_{10}(K_p)$ is given). We considered the developed CG model behaviour to be acceptably close to this quite hydrophilic range and, therefore, the Toc CG topology was added to the peptide model.

Morphological and biophysical characterization of peptide nanoparticles

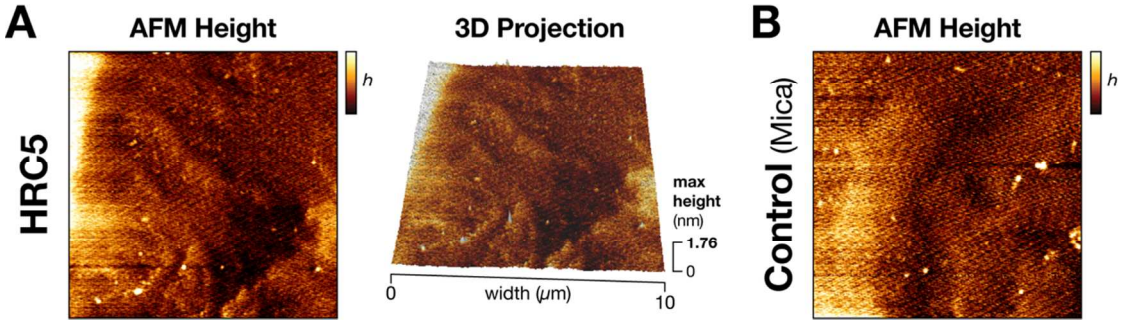

Figure S3 – AFM of mica surfaces pre-treated with HRC5. (A) Representative AFM image (10x10 μm) of freshly cleaved mica pre-incubated with HRC5 (30 μM) for 2 h and respective 3D projection. After screening of multiple sample areas, no deposited nanoparticles (NP) were detected. A 1.76 nm maximum height was reported during topographic imaging. The experiment was replicated in three independent days. A 24 h HRC5 incubation time was also tested, with similar results (data not shown). **(B)** Control AFM image (10x10 μm) of a freshly cleaved mica surface pre-incubated with sample buffer for 2 h. *h* – height

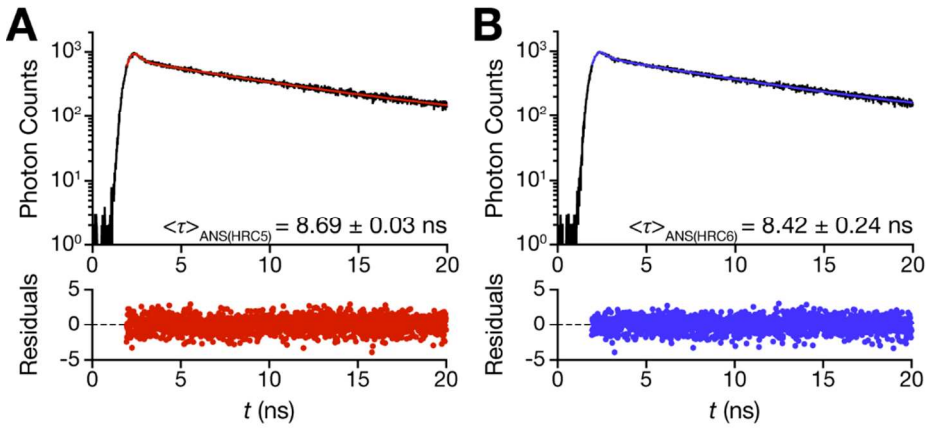

Figure S4 – Fluorescence intensity lifetime decays of ANS inserted in HRC5 (A) and HRC6 (B) NP. ANS (12.8 μM) was pre-incubated with either HRC5 or -6 NP (30 μM) for 10 min before performing measurements, to allow efficient insertion into the NP. Lifetime decays (0-20 ns) were collected with a standardized 10^3 photon count limit. Red and blue lines correspond to the best fit of a bi-exponential curve to fluorescence decays of ANS inserted in HRC5 or -6 NP, respectively. The respective residuals plots are represented. The presented results are one of three independent replicates.

Peptides sensitivity to trypsin proteolytic digestion

To study peptides' sensitivity to proteolytic digestion, trypsin (Gibco, Thermo-Fisher, Waltham, MA, USA) and HRC5 and HRC6 peptide samples were prepared in 10 mM HEPES, 150 mM NaCl, pH 7.4, from stock solutions. Samples were pre-incubated at 37 ºC for 5 min. Reaction mixtures composed of trypsin (20 µg/mL) and each peptide (30 µM) were prepared by adding trypsin to peptide samples. Peptide proteolytic digestion was quenched at specific time points (10 – 60 min) by diluting 10 µL of each peptide reaction mixture in 20 µL of non-reducing Laemmli's SDS sample buffer. For controls, peptide and trypsin samples were directly diluted into the same SDS sample buffer. Samples were boiled for 5 min at 99 ºC and centrifuged for 30 s at 2.5 rcf, before loading 15 µL on a 4-15% Tris-Glicine gel. The PageRuler™ (Thermo-Fisher) protein ladder was included in each gel as a molecular weight standard. The SDS-PAGE was run at constant 140 V. After completion, gels were immediately stained using a combined Coomassie Brilliant Blue G-250 (Biorad, Hercules, CA, USA) and EZBlue™ (Sigma) staining, as recommended by the providers. Peptide band densitometry was analyzed using the image processor Fiji.[21]

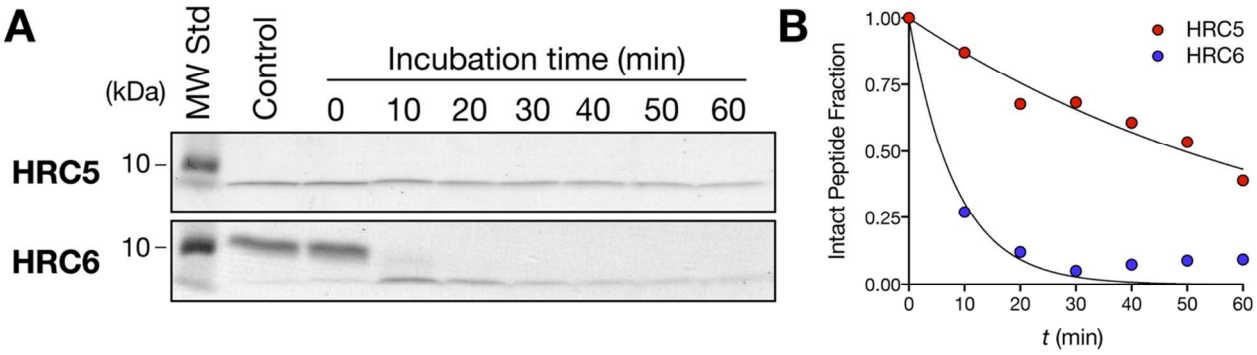

Figure S5 – Protease sensitivity of HRC5 and HRC6 peptides NP. (A) SDS-PAGE of HRC5 and HRC6 peptides samples (30 µM) incubated with trypsin (20 µg/mL). Incubations were performed at 37 ºC, collected at multiple time points, from 0 to 60 min, and subjected to non-reducing SDS-PAGE. A molecular weight standard was included in the first lane of each gel. Control samples correspond to peptide in the absence of trypsin. **(B)** Densitometry analysis of intact peptide content in each sample, measured from gel images, and normalized to the control in the absence of peptide digestion. A single exponential decay curve was fitted by non-linear regression to the experimental data sets to determine the respective peptide half-life ($t_{1/2}$). The $t_{1/2}$ of HRC5 and HRC6 proteolytic digestion were 49.5 min and 5.9 min, respectively.

References

(1) Lambert, D. M.; Barney, S.; Lambert, A. L.; Guthrie, K.; Medinas, R.; Davis, D. E.; Bucy, T.; Erickson, J.; Merutka, G.; Petteway, S. R. Peptides From Conserved Regions of Paramyxovirus Fusion (F) Proteins Are Potent Inhibitors of Viral Fusion. *Proc. Natl. Acad. Sci. U. S. A.* **1996**, *93*, 2186–2191.

(2) Pessi, A.; Langella, A.; Capitò, E.; Ghezzi, S.; Vicenzi, E.; Poli, G.; Ketas, T.; Mathieu, C.; Cortese, R.; Horvat, B.; Moscona, A.; Porotto, M. A General Strategy to Endow Natural Fusion-Protein-Derived Peptides with Potent Antiviral Activity. *PLoS ONE* **2012**, *7*, e36833.

(3) Figueira, T. N.; Palermo, L. M.; Veiga, A. S.; Huey, D.; Alabi, C. A.; Santos, N. C.; Welsch, J. C.; Mathieu, C.; Horvat, B.; Niewiesk, S.; Moscona, A.; Castanho, M.A.R.B.; Porotto, M. *In Vivo* Efficacy of Measles Virus Fusion Protein-Derived Peptides Is Modulated by Properties of Self-Assembly and Membrane Residence. *J. Virol.* **2017**, *91*, e01554.

(4) Jones, D. T. Protein Secondary Structure Prediction Based on Position-Specific Scoring Matrices. *J. Mol. Biol.* **1999**, *292*, 195–202.

(5) Buchan, D. W. A.; Minneci, F.; Nugent, T. C. O.; Bryson, K.; Jones, D. T. Scalable Web Services for the PSIPRED Protein Analysis Workbench. *Nucleic Acids Res.* **2013**, *41*, W349–W357.

(6) Gasteiger, E.; Hoogland, C.; Gattiker, A.; Duvaud, S.; Wilkins, M. R.; Appel, R. D.; Bairoch, A. *Protein Identification and Analysis Tools on the ExPASy Server*; Humana Press: Totowa, NJ, 2005; pp. 571–607.

(7) Gautier, R.; Douguet, D.; Antonny, B.; Drin, G. HELIQUEST: a Web Server to Screen Sequences with Specific Alpha-Helical Properties. *Bioinformatics* **2008**, *24*, 2101–2102.

(8) Zhang, Y. I-TASSER Server for Protein 3D Structure Prediction. *BMC Bioinf.* **2008**, *9*, 40.

(9) Roy, A.; Kucukural, A.; Zhang, Y. I-TASSER: a Unified Platform for Automated Protein Structure and Function Prediction. *Nat. Protoc.* **2010**, *5*, 725–738.

(10) Yang, J.; Yan, R.; Roy, A.; Xu, D.; Poisson, J.; Zhang, Y. The I-TASSER Suite: Protein Structure and Function Prediction. *Nat. Methods* **2015**, *12*, 7–8.

(11) Pettersen, E. F.; Goddard, T. D.; Huang, C. C.; Couch, G. S.; Greenblatt, D. M.; Meng, E. C.; Ferrin, T. E. UCSF Chimera--a Visualization System for Exploratory Research and Analysis. *J Comput Chem* **2004**, *25*, 1605–1612.

(12) Hanwell, M. D.; Curtis, D. E.; Lonie, D. C.; Vandermeersch, T.; Zurek, E.; Hutchison, G. R. Avogadro: an Advanced Semantic Chemical Editor, Visualization, and Analysis Platform. *J. Cheminf.* **2012**, *4*, 17.

(13) Schmid, N.; Eichenberger, A. P.; Choutko, A.; Riniker, S.; Winger, M.; Mark, A. E.; van Gunsteren, W. F. Definition and Testing of the GROMOS Force-Field Versions 54A7 and 54B7. *Eur. Biophys. J.* **2011**, *40*, 843–856.

(14) Melo, M. N.; Ingólfsson, H. I.; Marrink, S. J. Parameters for Martini Sterols and Hopanoids Based on a Virtual-Site Description. *J. Chem. Phys.* **2015**, *143*, 243152.

(15) Feenstra, K. A.; Hess, B.; Berendsen, H. Improving Efficiency of Large Time-Scale Molecular Dynamics Simulations of Hydrogen-Rich Systems. *J. Comput. Chem.* **1999**, *20*, 786–798.

(16) Bulacu, M.; Goga, N.; Zhao, W.; Rossi, G.; Monticelli, L.; Periole, X.; Tieleman, D. P.; Marrink, S. J. Improved Angle Potentials for Coarse-Grained Molecular Dynamics Simulations. *J. Chem. Theory. Comput.* **2013**, *9*, 3282–3292.

(17) Marrink, S. J.; Risselada, H. J.; Yefimov, S.; Tieleman, D. P.; de Vries, A. H. The MARTINI Force Field: Coarse Grained Model for Biomolecular Simulations. *J. Phys. Chem. B* **2007**, *111*, 7812–7824.

(18) Bussi, G.; Donadio, D.; Parrinello, M. Canonical Sampling Through Velocity Rescaling. *J. Chem. Phys.* **2007**, *126*, 014101.

(19) Berendsen, H.; Postma, J.; van Gunsteren, W. F.; DiNola, A.; Haak, J. R. Molecular-Dynamics with Coupling to an External Bath. *J. Chem. Phys.* **1984**, *81*, 3684–3690.

(20) Shirts, M. R.; Chodera, J. D. Statistically Optimal Analysis of Samples From Multiple Equilibrium States. *J. Chem. Phys.* **2008**, *129*, 124105.

(21) Schindelin, J.; Arganda-Carreras, I.; Frise, E.; Kaynig, V.; Longair, M.; Pietzsch, T.; Preibisch, S.; Rueden, C.; Saalfeld, S.; Schmid, B.; Tinevez, J.-Y.; White, D. J.; Hartenstein, V.; Eliceiri, K.; Tomancak, P.; Cardona, A. Fiji: an Open-Source Platform for Biological-Image Analysis. *Nat. Methods* **2012**, *9*, 676–682.